

United Nations Educational Scientific and Cultural Organization
and
International Atomic Energy Agency

THE ABDUS SALAM INTERNATIONAL CENTRE FOR THEORETICAL PHYSICS

**WIDEBAND SIMULATION OF EARTHQUAKE GROUND MOTION
BY A SPECTRUM-MATCHING, MULTIPLE-PULSE TECHNIQUE**

Alexander Gusev¹

*Institute of Volcanology and Seismology FEB RAS,
9 Piip Blvd, 683006 Petropavlovsk-Kamchatskii, Russian Federation
and
The Abdus Salam International Centre for Theoretical Physics, Trieste, Italy*

and

Victor Pavlov²

*Kamchatka Branch, Geophysical Service RAS,
9 Piip Blvd, 683006 Petropavlovsk-Kamchatskii, Russian Federation
and
The Abdus Salam International Centre for Theoretical Physics, Trieste, Italy.*

MIRAMARE – TRIESTE

April 2006

¹ gusev@emsd.iks.ru

² pvm@emsd.iks.ru

Abstract

To simulate earthquake ground motion, we combine a multiple-point stochastic earthquake fault model and a suite of Green functions. Conceptually, our source model generalizes the classic one of Haskell (1966). At any time instant, slip occurs over a narrow strip that sweeps the fault area at a (spatially variable) velocity. This behavior defines seismic signals at lower frequencies (LF), and describes directivity effects. High-frequency (HF) behavior of source signal is defined by local slip history, assumed to be a short segment of pulsed noise. For calculations, this model is discretized as a grid of point subsources. Subsource moment rate time histories, in their LF part, are smooth pulses whose duration equals to the rise time. In their HF part, they are segments of non-Gaussian noise of similar duration. The spectral content of subsource time histories is adjusted so that the summary far-field signal follows certain predetermined spectral scaling law. The results of simulation depend on random seeds, and on particular values of such parameters as: stress drop; average and dispersion parameter for rupture velocity; rupture nucleation point; slip zone width/rise time, wavenumber-spectrum parameter defining final slip function; the degrees of non-Gaussianity for random slip rate in time, and for random final slip in space, and more. To calculate ground motion at a site, Green functions are calculated for each subsource-site pair, then convolved with subsource time functions and at last summed over subsources. The original Green function calculator for layered weakly inelastic medium is of discrete wavenumber kind, with no intrinsic limitations with respect to layer thickness or bandwidth. The simulation package can generate example motions, or used to study uncertainties of the predicted motion. As a test, realistic analogues of recorded motions in the epicentral zone of the 1994 Northridge, California earthquake were synthesized, and related uncertainties were estimated.

1. INTRODUCTION

Despite many studies addressed at the simulation of ground motion from a large earthquake, much is still to be done. In general, to simulate earthquake ground motion from a known fault, one should be capable to simulate both (1) fault/source space-time evolution, and (2) wave propagation from fault to receiver. The last step may include such separate substeps as (2a) propagation of linear wave up to the bedrock under the site/receiver, and (2) non-linear propagation in weaker upper layers. We confine our study by (1) and (2a); moreover, in (2a) we use simple, horizontally layered, model of Earth structure.

As for emulation of space-time source evolution, two general approaches have been developed up to present. One is based on an elastodynamic representation of a fault, and treats a fault as a dislocation/crack. While this model is conceptually attractive, in most its realizations it fails to predict an important property of the fault motion – localization of slip process in a narrow running strip (Haskell 1964, 1966; Heaton 1990). It also cannot predict realistically entire wide-band spectrum of source radiation. Another approach is to use semi-empirical models that incorporate some theoretical reasoning with generalization of empirical data. In this line, most important steps are: Haskell (1966)-Aki (1967) concept of approximate self-similitude of earthquake sources and of spectral scaling law; Aki (1967)-Brune (1970) proposal of simple omega-square spectral scaling law with self-similitude; demonstration of lack of self-similitude in wideband spectral scaling (Gusev 1983); derivation of properties and parameters of strong motion based on spectral scaling law, both assuming similitude and using point source model (Hanks and McGuire 1981, Boore 1983) and assuming wideband semi-empirical finite source models with no spectral similitude (Gusev 1983, Papageorgiou and Aki 1983, 1985, Gusev 1989). (Spectral similitude means that after appropriate scaling, mean spectral shape is identical at any Mo.) Many efforts were spent to understand how to compose small earthquake records into a record of a large one (Boatwright 1982, Papageorgiou and Aki 1983, Koyama 1985, Irikura 1986, and later work). Note that this entire line of study is based on the assumption that such composition is a meaningful, disputable issue from a tectonophysical viewpoint. For fault-to-site distances comparable or exceeding fault width, these approaches have produced a number of useful techniques for ground motion simulation. Some of them use a systematic model-based derivation (like Boore 1983 or Papageorgiou and Aki 1983), other propose rules how to derive large event record from observed records of small events (“empirical Green function method”, Hartzell 1978, Irikura 1986). However, these approaches essentially fail to solve the problem of prediction of ground motion at small distances where realistic details of space-time evolution of a large event become critical. The model of Gusev (1989) gave some hope in this respect, but was never developed into a practical simulator.

The main difficulty, in our view, is the need to comply simultaneously with the two critical requirements: (1) low-frequency component of simulated signal must incorporate our knowledge of details of real fault propagation, first of all the running strip model of Heaton (1990) and final slip structure anticipated by Andrews 1980 and refined by Somerville et al. (1999); (2) high-frequency component is to

follow our empirical knowledge of typical Fourier spectra at moderate-to-large distances, and also to emulate non-Gaussian amplitude statistics of observed near-fault records (Gusev 1996). Our approach, presented below, is aimed to satisfy, systematically, both these groups of requirements. This is performed in two consecutive steps: first we generate a source with unrealistic, nearly-white-noise high-frequency signal but accounting for all important details of low-frequency behavior, of envelope structure and of statistics of peaks; then we smooth the source signal in an accurately controllable manner, fitting an empirical spectral scaling law (i.e., in essence, an empirical acceleration spectral trend).

The simulation procedure employed is aimed at a realistic prediction of earthquake ground motion for the magnitude range $M_w=5-9$, hypocentral distance range 5-400 km and frequency band 0.03-25 Hz. The earthquake source is represented as a set of point sources with appropriate time histories. For any site in question, and for each subsource, we calculate medium response to a unit step in seismic moment for a point dislocation (further referred as “Green function” in the loose sense) and convolve it with the respective time history. Such contributions of all subsources are added up to a synthetic ground motion. Correspondingly, the entire simulator procedure consists of the source simulator module, Green function calculator module, and the convolver module that performs convolution in time, and summation over subsources. We use an original Green function calculator for layered medium, accurate over entire relevant frequency band, from static terms (“swing”) to very high frequencies.

To illustrate capabilities of the proposed method we simulate near-source ground motion of a well-recorded earthquake, and analyze the uncertainty of the simulation.

2. THE TECHNIQUE FOR THE SIMULATION OF STRONG GROUND MOTION

2.1 Source simulator

The source simulator algorithm generalizes the classic Haskell (1966) stochastic fault model (that, in turn, adds randomness to the better-known rectangular fault of Haskell (1964). Haskell (1966) assumes that at a particular point, the process of slip is of definite duration, denoted “rise time”. He also proposed that the slip velocity, viewed as a function of space and time, is a random function. We follow these two assumptions, but introduce the following modifications:

1. Instead of the Haskell’s fault with a constant final slip, a variable, random final slip is assumed, governed by the power spectrum that is a power-law with respect to wavenumber. This kind of wavenumber spectrum was proposed by Andrews (1980) and confirmed by Somerville et al. (1999) based on empirical data.
2. Kinematics of Haskell’s source is generalized in the following way: the rupture front is of a general shape (not a straight line); the nucleation point is arbitrary; and the rupture velocity is variable, with a prescribed mean (not a constant).

3. Instead of Haskell's omega-cube far field spectrum, the far-field spectrum of a simulated source is adjusted, in its high-frequency part, to a particular spectral shape derived from a preset regional spectral scaling law.

This general concept is to be realized in a numerical scheme. Following in many respects (Gusev 1983) we introduce a grid of point-like dislocation subsources. Each subsurface possesses a fraction of the total seismic moment of the source, and the distribution of seismic moment over subsources is governed by the aforementioned random final slip function. The duration of a subsurface is defined first of all by the value of rise time (duration of local slip), assumed the same over entire fault in the current version of the algorithm. The duration is somewhat increased additionally, to account for the finite size of the fault cell represented by a point subsurface.

Each subsurface has an individual, random moment rate time history. In absolute time, subsources are switched on by the arrival of the rupture front, otherwise their time histories are uncorrelated. At present, we ascribe no direct physical meaning to individual point subsources; they serve only as a tool for numerical simulation of an incoherent source with mostly uncorrelated spots. The number of subsources can be large (50x25 grid is quite acceptable). However, the assumed complete lack of correlation among time histories of subsources may become inadequate for a very dense grid. For this reason, the model may overpredict high-frequency amplitudes when used at a too small distance from a fault. A rough estimate of the minimum fault distance is about (fault length)/20, or 5 km for a 100-km fault.

The above considerations led us to the simulation procedure that consists of the following steps:

1. **Specification of parameters of the model.** These include common source parameters like seismic moment, stress drop, nucleation point, rise time and mean rupture velocity. Source shape is assumed to be rectangular, length $L \times$ width W . The values of L and W can be either preset or calculated from $L(M_w)$ correlation relationship adjusted for stress drop, and using M_w -dependent aspect ratio. Also, parameters of numerical model are set, namely: the subsurface numbers along L and W , and time step. In the current version, subsurface strike, dip and slip are identical. Values of other parameters, listed below, are also selected at this stage.

2. **Monte-Carlo simulation of the final slip distribution.** This simulation departs from generating 2D random white Gaussian spectrum that represents logarithm of slip in wavenumber domain. Then the power-law filter is applied; its exponent s is preset. The result is passed to coordinate domain, and re-scaled to acquire the preset value of rms deviation, equal to CV_{xy} . Then, the obtained function is exponentiated, resulting in everywhere positive random function with lognormally distributed values. At last, a finite portion of the produced 2D field is cut out by an appropriate 2D taper ("cap") function, nonzero over a L by W rectangle. The value of CV_{xy} defines how heavy tails shall have the distribution of values of the simulated final slip function. At $CV_{xy}=0$, the constant-final-slip case is simulated. Tech-

nically, CV_{xy} is, approximately, the coefficient of variation for slip values. When the source side cuts the free surface, tapering is switched off along it. For an example of simulated final slip distribution see Fig. 1.

3. Monte-Carlo simulation of the rupture propagation history. In the simplest mode, rupture front is assumed to be circular and to move in steps of identical length, smaller than the size of a subsource cell. At the i -th step, the value v_i of rupture velocity is determined as a product of the preset mean value v_m , and of a random a random number drawn from uniform distribution in the range $(1-DV, 1+ DV)$, where DV is another preset parameter. In a more advanced mode, 2D distribution of random values of rupture velocity controls the front propagation history. For an example of simulated rupture front propagation see Fig. 1.

4. Monte-Carlo simulation of “skeleton” time histories of each subsource. These “skeleton” time histories for moment rate functions are generated as random sequences of delayed positive delta-like pulses (spikes), with appropriate amplitude and delay statistics, and essentially represent segments of (modulated) white noise with positive mean. The delays of pulses are simulated so as to make their time sequence nearly Poissonian. The amplitude statistics of spikes is lognormal. By selection of the coefficient of variation CV_i that is the parameter of the lognormal law, one can define whether the output accelerograms will appear like Gaussian noise or will be non-Gaussian and look “spiky” to some (controllable) degree. For a certain subsource, the onset time of the sequence is determined by the arrival time of the rupture front to this subsource. The duration of the sequence is determined by the value of

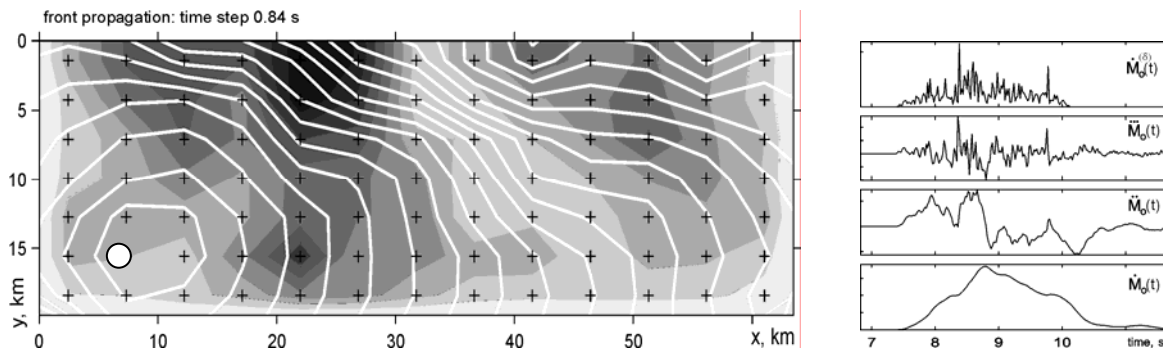


Figure 1: An example of 2D final slip function, shown as density. Fault parameters: $M_w=7.2$, $L = 63$ km, $W=20$ km. Subsource grid 13×7 , subsource size 4.8×2.9 km. Random slip follows isotropic $k^{-1.5}$ wavenumber amplitude spectrum. Note the effect of 2D taper function over three sides; upper side ($y=0$) assumed to cross the Earth surface. White dot is the nucleation point. White contours are successive rupture front positions, simulated kinematically from random rupture velocity field. Crosses are positions of point subsources.

Figure 2: Time histories associated with a particular subsource ($i_x=4$, $i_y=1$) in the earthquake source of Fig. 1. Skeleton time history is the upper trace. Three other traces are third, second and first time derivatives of $M_0(t)$; they represent subsource contribution to far-field body wave acceleration, velocity and displacement, respectively.

the rise time. From the tectonophysical viewpoint, each delta-like spike can be related to a failure of a single small asperity, in accordance with (Gusev 1989). The heavy-tailed statistics of spike amplitudes

is needed to emulate heavy-tailed, non-Gaussian statistics of acceleration peaks (Gusev 1996); such a behavior is presumably the manifestation of the heavy-tailed distribution of the fault strength and local stress drop. The complete set of “skeleton” time histories of subsources represents a “skeleton source”. For an example see Figs. 2 and 3.

5. Creating the “dressing operator”. At this point, low-frequency and low-wavenumber behavior of the source is already constructed. As for high-frequency radiator, its envelope and peak statistics have also been simulated. The only problem is the unrealistic spectral behavior at high frequencies (that is, at frequencies $(4-6) \times (\text{corner frequency})$ and above). To rectify this deficiency, we apply to skeleton time functions a specially designed “dressing operator”. In time domain, it is represented by a pulse with unit integral, or, shortly, “unit pulse”. To construct the dressing operator we first calculate the source spectrum (Fourier spectrum of the moment rate time history of an equivalent point source) that corresponds to the time history of constructed “skeleton” source (obtained by stacking all subsources). We then compare the result with the preset “target” source spectrum derived from the regional spectrum scaling law (that is, ultimately, from averaged observed spectra) for the given values of moment magnitude and stress drop. The ratio of these spectra, smoothed and somewhat modified, gives us the module of sought operator in frequency domain. Its phase spectrum is adjusted so as to make its time-domain representation a minimum-phase pulse. This procedure is illustrated on Fig. 4.

6. “Dressing the skeleton”. The dressing operator (i.e., convolution with unit pulse) is applied to “skeleton” time histories of subsources, giving a final set of individual moment rate time histories of subsources. The spectrum of their sum, in its high-frequency part, approximates the “target” spectrum in the rms sense. The same sum in time domain gives the shape of the far-field body wave displacement signal for a ray normal to the fault. Similarly, using in convolution first and second derivatives of unit pulse (seen in Fig. 4); one obtains the shapes of far-field velocity and acceleration signals, as illustrated in Fig. 2.

The described source simulation algorithm is capable of producing realistically-looking far-field and near-field ground motions. In particular, it reproduces well the common directivity effects (see Fig. 5). Also, it successfully emulates, in terms of amplitude levels, observed peak accelerations and velocities, as well as response spectra and characteristic durations. However, the described procedure has a significant deficiency: its repeated runs generates signals whose amplitudes and response spectral levels vary only slightly from run to run. The cause is that simulated source spectrum occurs to be too close to the mean/target spectrum, because of the feedback loop built into the described procedure. Indeed, it is designed to provide, approximately, a preset level of mean far-field Fourier spectrum amplitudes at each frequency. This requirement might be acceptable for the special case of a single simulation run. However, the mentioned feedback strongly dampens the natural variability of signals: output spectral amplitudes generated in successive runs of the procedure are automatically kept within an unrealistically narrow corridor. The nearly-perfect spectral fit that is seen on Fig. 4c illustrates this problem.

Therefore, we must disconnect the feedback loop to reproduce realistically the random variability of ground motion.

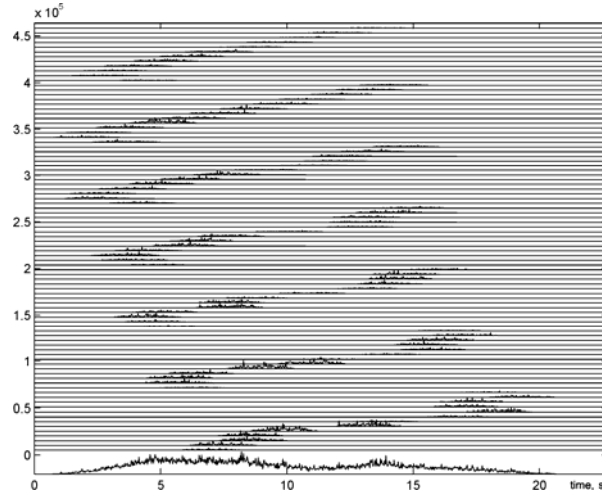


Figure 3: Skeleton time histories for 91 subevents of the source of Fig. 1. The lowermost trace is the sum over subsources.

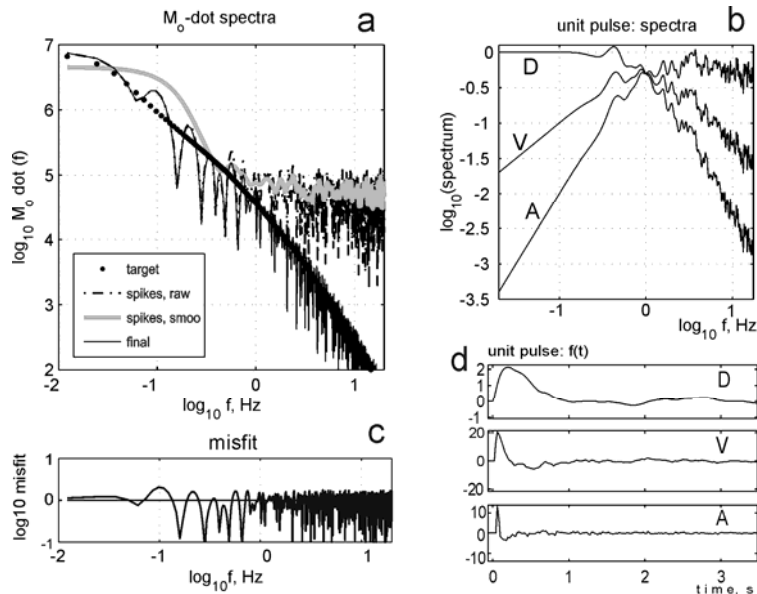


Figure 4: Spectral fitting for the example case of Fig 1,3. a: a set of $\dot{M}_0(t)$ spectra (in 10^{20} dyne cm units) that represent: target spectrum, spectrum of the skeleton time function (sequence of spikes), its smoothed version, and final spectrum. b: Amplitude spectra for correction operator or unit pulse; multiplication by spectrum D converts skeleton spectrum to final $\dot{M}_0(t)$ spectrum, spectra V and A , similarly, perform conversion to $\ddot{M}_0(t)$ and $\dot{M}_0(t)$. Spectrum D is obtained by division of target spectrum of graph a by smoothed skeleton spectrum, and set to unity at frequencies above $0.2 \times$ (corner frequency). c: spectral misfit between target spectrum and final spectrum of graph a. Note that spectral fit is unrealistically good in this particular simulation. d: time function representation of the correction operator or unit pulse, see graph b for amplitude spectra. Phases of pulses in d are from the “minimum-phase” constraint.

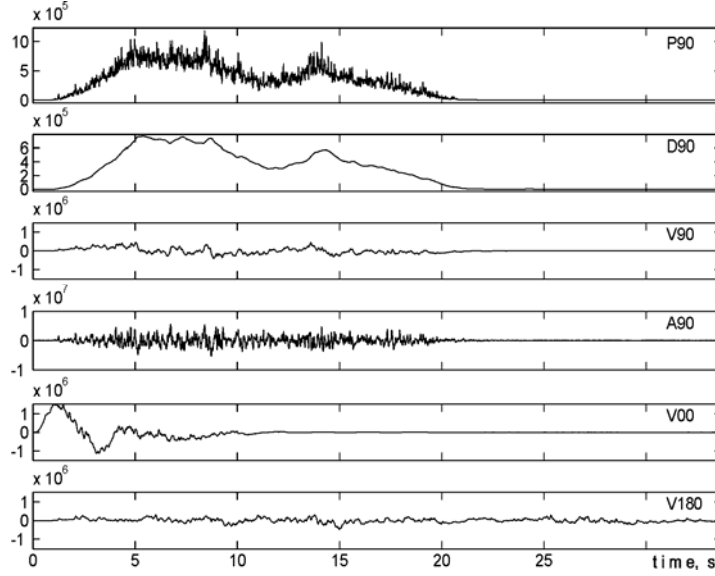


Figure 5. “Source time functions” for the example of Fig1-4. P90: skeleton time function reproduced from Fig A3. D90, V90 and A90 are traces for $\dot{M}_0(t)$, $\ddot{M}_0(t)$ and $\ddot{M}_0(t)$, obtained by summation of subsurface signals without relative delay. Their shape is identical to far-field body wave signals as observed on the ray normal to the fault. Two additional “velocity” signals V00 and V180 are obtained by phase-delayed summation of S-waves from subsources. They correspond to observers positioned along directions “forward” (+x) and “backward” (-x) with respect to main rupture propagation; these signals illustrate directivity or “Doppler effect”

Towards this end, the above algorithm was modified in the following way. Instead of calculating the spectral correction operator of the Step 5 through individual fit at each simulation run, it is calculated only once. On a preliminary stage, changing only the random seeds, we repeat the simulation many (25) times with all parameters fixed, and then average the (amplitude) spectral correction functions obtained in each run. From this average spectral correction we construct a “mean” correction operator, and “freeze” it. Afterwards, simulation proper is performed, single or multiple, with “frozen” correction operator and no feedback. After such a modification, the algorithm generates signals with realistic variability. These are adequate for such uses as: generating suites of design earthquake ground motion, studying its sensitivity to variations of input parameters of the model, and/or analyzing variability/uncertainty of the result.

2.2 Green function calculator, convolution module and attenuation correction

To match the level of accuracy promised by the source simulator described above, an accurate wide-band Green function calculator was needed. We use an original discrete wavenumber code that calculates pulse response of the layered elastic medium for a step-like double-couple source. The code is based on the advanced version of the method of Alekseev and Mikhailenko (1980), recently developed by Pavlov (2001). Following Takeuchi and Saito (1972) the solution is initially represented, in cylindrical coordinates, as an integral sum over surface vector harmonics. Alekseev and Mikhailenko (1980) introduce a distant boundary and convert the integral representation into a series over discrete

wavenumbers that are roots of a certain equation related to Bessel functions. To determine coefficients of this series, for each frequency-wavenumber pair one must solve ordinary differential equations in depth coordinate (a single equation for the SH case and a pair of coupled equations for the P-SV case). Right-hand parts of these equations are corresponding coefficients for the expansion of the point source. These differential equations are solved analytically by means of the “auxiliary functions” first introduced by Fatyanov and Mikhailenko (1988). For SH waves, an auxiliary function is the scalar function of depth such that the depth derivative of the SH potential is equal to the product of the auxiliary function and the potential. For the P-SV case, the auxiliary function is similar and forms a 2x2 matrix. Auxiliary functions and displacement and stress coefficients are calculated by closed analytical formulas. The main advantage of this method is the lack of numerical instability inherent within propagator methods, because in the auxiliary function method all relevant exponential factors are below unity by absolute value. To ensure preset uniform numerical accuracy, the number of terms in the series expansion is selected adaptively. The developed numerical method provides accurate broad-band representation of ground motions in a layered medium. It has no intrinsic limitations with respect to layer thickness and bandwidth, and predicts both so named “swing effect” at zero frequency, and high-frequency body wave spikes equally well.

In the convolution module, the first step is to convolve over time the subsurface time histories and the corresponding subsurface Green functions for a certain site. The second step is to add thus obtained contributions of all subsources, resulting in the ground motion at the site. This is repeated for each site. In addition, attenuation corrections (through “kappa” factor and distance-dependent term) are added here. Alternatively, frequency-independent Q profile can be included in the main procedure for Green function calculation. The option of frequency-dependent Q profile is under development.

2.3 Parameters of the model

We give below the list of most important parameters that define a particular realization of our numerical model. Parameters can be selected/modified to attain such aims as: (1) tuning both the source model and the model of the medium to a particular seismological situation; in order to tune the model, particular values of parameters are selected; and (2) for analyzing the variability of the predicted motion, both random and parameter-related. In particular, random variability (a component of aleatoric uncertainty) related to intrinsically stochastic part of the model is simulated by using a series of sets of random seeds. As for dealing with random variability (again aleatoric) related to the natural variability of input parameters, there are two ways. The less general way, efficient even in cases of expressed non-linearity, is to generate a set of random values of one or more input parameters (by drawing random numbers out of appropriate random distribution(s)), and to use these input parameters for a series of simulations. Another, more general but less reliable approach is to derive distribution of output parameter from those of input parameters, using sensitivity. That is, aleatoric rms uncertainty in ground motion parameter “ a ” with respect to variation of some input parameter “ b ” is determined by the product of sensitivity

of “ a ” with respect to “ b ”(i.e., merely, derivative da/db), and assumed rms error that describes natural variability in “ b ”. This simple procedure is completely justified only for cases of weak nonlinearity and independent parameters. As for epistemic uncertainty in “ a ” that reflects limits of our knowledge of “ b ”, it can be determined again via sensitivity, only instead of rms error in b one should use its range or tolerance that define input uncertainty of “ b ”. In this manner, both aleatoric and epistemic uncertainty can be estimated. One more use of selection and variation of input parameters is the generation of a suite of representative ground motions. Note that just the analysis of uncertainty can give us a clear idea which variants can be considered “representative”.

In the following we list the most important parameters, divided in three groups.

A. Parameters of the earthquake source/fault and of regional seismicity (in general, or for its emulated subset)

1. “Geometry”

1.1. Fault rectangle center geographic coordinates (shortly, “epicenter”)

1.2. Fault rectangle center depth h

1.3. Strike, dip and rake angles

1.4. Length L and width W of the fault rectangle

1.5. Numbers of subsources: n_L along L and n_W along W

2. “Kinematics”

2.1. Location of the nucleation point x_{nuc} , y_{nuc} along L and W ,

2.2. Half-ranges dL and dW of subsource center random perturbation along L and W

2.3. Rupture velocity parameters: mean value v_m , half-range dvr of random perturbation of mean value of rupture velocity; relative range DV of random perturbation of instant value of rupture velocity

2.4. Rise time T_{rise}

3. “Dynamics”

3.1. Moment magnitude M_w .

3.2. Stress drop, relative value with respect to regional average.

3.3. CV_r parameter that defines the degree of non-Gaussian behaviour (“spikyness”) of accelerograms.

3.4. CV_{xy} parameter that defines how strongly oscillating (non-Gaussian) will be the simulated final slip function.

3.5. The exponent s in the power law that defines the power spectrum ($\propto k^{-s}$) of the final slip.

4. Random seeds

4.1. Random seed defining the final slip function.

4.2. Random seed defining the time series of subsources.

4.3. Random seed defining the perturbation of the mean value of rupture velocity.

4.4. Random seed defining the random history of rupture velocity

4.5. Random seed defining the perturbation of nucleation point position.

5. A particular scaling law ($M_0(f | M_w)$) for source spectra, tabulated or in an analytical form.

In the case of a non-standard value of stress drop, spectral scaling law is modified correspondingly. To derive this modification, we use the logarithmic deviation δ of stress drop value from its regional average ($\delta = \Delta \log \Delta \sigma$). In the present version of the algorithm, two particular spectral shapes are preset: for W.USA shallow earthquakes, Joyner (1984) modification of Brune (1970) scaling law (assuming similitude); and semi-empirical scaling law of Gusev (1983), assuming lack of similitude.

B. Parameters of the layered medium and of a site.

1. The site position
2. The velocity-density column for a site (includes top depth, VP, VS, and maybe QP and QS for each layer.
3. The value of kappa parameter for a site (site-specific upper layer attenuation contribution), and Q(f) vs. distance, if needed.

3. AN EXAMPLE CASE: NORTHRIDGE 1994 EARTHQUAKE

3.1 General issues

An appropriate test for the algorithm described above is its application for emulation of a series of records obtained in the epicentral zone of a large earthquake on various ground types. To perform such a test, 18 near-source records of $M=6.7$, 1994, Northridge, California, earthquake were simulated. To fix the parameters of the model we widely used the published results of source inversion after Wald et al. (1996), listed below. The only parameter whose values were fit to real data is the kappa parameter.

Wald et al. (1996) give structure description for “rock” and “soil” medium structures. We used them for stations whose ground was specified as “rock” and “deep soil”/“basin”. For intermediate ground conditions, we introduced also the “intermediate” structure with the velocity profile “interpolated” between the former two; it was used for two stations that were specified neither as rock nor as deep soil / basin ones. For the general overview of the fault and stations see Fig. 6.

3.2 Assumed values for parameters that were used for simulation

Most of the following parameters are adapted from (Wald et al., 1996). For other parameters, explanation is given in brackets.

Fault center: $\varphi=34.28^\circ$; $\lambda=-118.56^\circ$; depth=12.5 km

Strike=122°; **dip**= 40°; **rake**=101°

Length $L=18$ km; **width** $W=24$ km.

Mean rupture velocity $v_m=3$ km/s;

Nucleation point position: $\varphi=34.35^\circ$ $\lambda=-118.54^\circ$ depth=17 km

Rise time $T_{rise}=0.7s$

Moment magnitude: $M_w=6.7$

Stress drop: 1.4 times above the regional average, or 75 bar in the Brune-Joyner spectral model. [Based on the Ward et al. (1996) figure of 74 bar for static stress drop]

Relative range for ν : $DV=0.8$ [A guess, our results suggest that it is somewhat too low]

CV_t parameter: 0.5 [Based on our experience with simulation. This is a reasonable trade-off between “dull” Gaussian-noise type accelerograms and expressedly non-Gaussian records with too many prominent individual spikes]

CV_{xy} parameter: 0.5 [Based on our experience with simulation, this is a reasonable trade-off between nearly-constant slip over the area ($CV_{xy}=0-0.2$) and slip functions with very expressed “asperities” generated at $CV_{xy}>0.8$]

The exponent s in the power law for the power spectrum of the final slip: 1.5 [Andrews (1980) proposed $s=2$ from self-similarity considerations; using this value results in seemingly too scarce high wavenumbers, this we somewhat decreased this value. The estimate of Somerville ($s=1.75$) is close to our assumption]

Scaling law of source spectra. For the particular case of Western USA, Brune’s omega-square law, in the modification of Joyner (1984), with “f-max” effect formed by the “kappa” factor after Anderson and Hough (1984).

Medium properties for stations. We give vertical profiles and kappa values used for particular sites/stations. Distance-dependent attenuation term was omitted in this simulation. Stations were divided into three groups: “rock”; “deep-soil/basin” and “intermediate”, see Table 1.

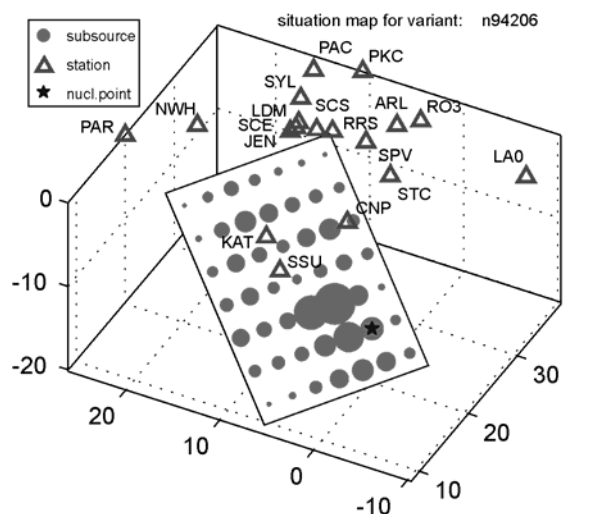


Figure 6. Perspective view of source rectangle and receivers/stations for the $M_w=6.7$ Northridge 1994 event. Sub-sources indicated as dots whose size reflects its seismic moment as used in the variant #206. Star is the nucleation point. Coordinates are in km.

Table 1. Vertical velocity-density profiles and kappa values

Layer top depth, km	Vp, km/s	Vs, km/s	Density, t/m ³	Kappa, s
<i>"Rock" profile</i>				
0.0	1.9	1.0	2.1	0.035
<i>"Basin" profile</i>				
0.0	0.8	0.3	1.7	0.075
0.1	1.2	0.5	1.8	
0.3	1.9	1.0	2.1	
<i>"Intermediate" profile</i>				
0.0	1.2	0.5	1.8	0.050
0.1	1.9	1.0	2.1	
0.3	3.8	1.5	2.2	
<i>all profiles</i>				
0.5	4.0	2.0	2.4	
1.5	5.5	3.2	2.7	
4.0	6.3	3.6	2.8	

3.3 Results of the simulation

As already was noted, only the site-related kappa values for each of the three groups of stations were adjusted during simulation. The selected values are within the typical range for site-related kappa. The value for basin stations looks somewhat too high, but we believe that this value is in fact in agreement with observations of enhanced nonlinear attenuation of large-amplitude waves in a softer ground. The fitting of any parameters, in particular, kappa values, in frames of an experiment aimed at verification of simulation technique, needs justification. In our view, for rock sites, or for prediction of bedrock motion, kappa could be estimated in advance from weak motion data. In fact, an a priori value of 0.04 s was used in our preliminary study quite successfully. For soil sites, however, kappa estimated from weak motion may be too low when used with strong motion. In these cases, certain adjustment seems acceptable.

To select an example of simulation, we had some freedom because we could try many variants of random seeds, and this fact may make our demonstration example less convincing. We can only mention that we actually looked through only ten variants, to select two ones numbered 206 and 300 that show ground motion parameters quite near to observed ones. See Fig. 7 for stacked source time functions of both variants. For variant #206, we show subsurface moment rate functions on Fig. 8, and compare simulated and observed time histories of ground motion at five representative stations on Fig. 9. To

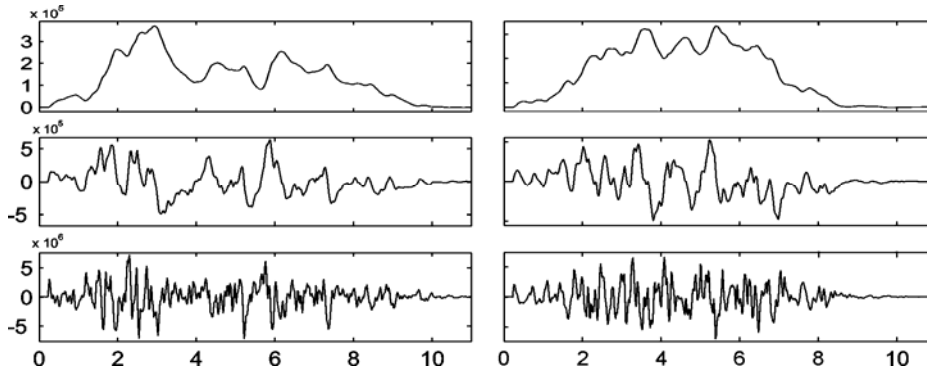


Figure 7. Far-field source time functions for the variants #206 (left) and #300 (right). Top to bottom: functions $\dot{M}_0(t)$ (moment rate), $\ddot{M}_0(t)$, and $\ddot{\ddot{M}}_0(t)$ in 10^{20} dyne cm/s, 10^{20} dyne cm/s², and 10^{20} dyne cm/s³ units.

generate the mentioned ten variants, we changed three random seeds that define: 2D final slip function, subsurface time functions, and rupture front time history, respectively.

Let us now consider the differences between simulated and observed time functions. We analyse these differences in the form of logarithmic amplitude misfit, denoted generally as $\Delta \log_{10}(A) = \log_{10}(A(\text{simulated})) - \log_{10}(A(\text{observed}))$. Misfit was determined for pseudo response acceleration PRA ($\Delta \log_{10}(\text{PRA})$) calculated over 25 frequencies that cover the 0.1-20 Hz range with an approximately constant step in log frequency; and also for peak amplitudes of acceleration, velocity and displacement,

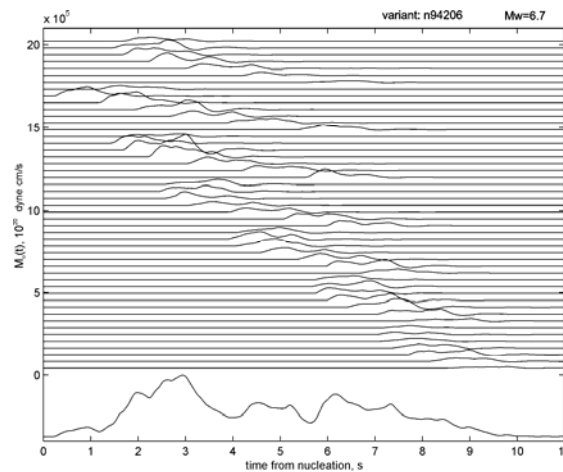


Figure 8. Moment rate time functions for 49 subsources of variant #206 of a simulated Northridge earthquake, and also the summary moment rate function (below).

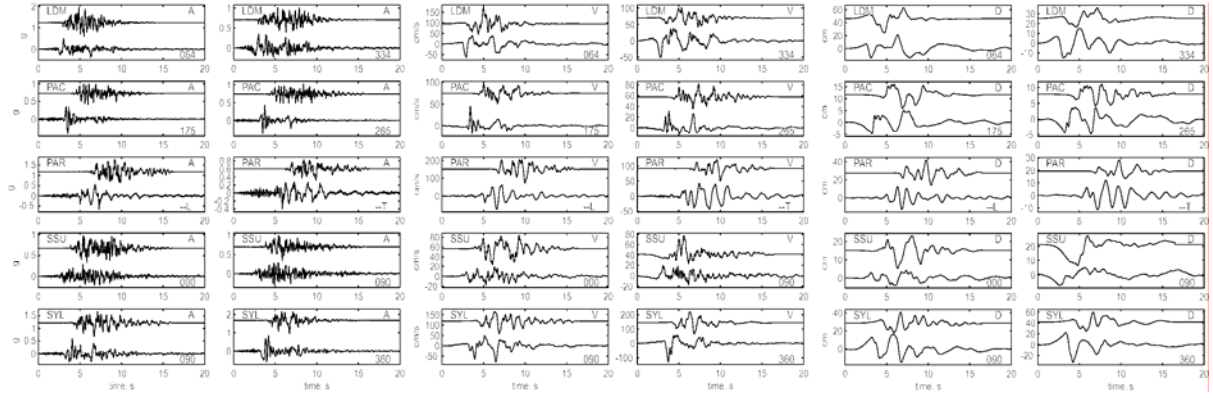


Figure 9. Comparison of observed and simulated (variant 206) time histories for acceleration (left), velocity (center) and displacement (right) for five stations, for two horizontal components. Simulated traces are rotated and band-filtered in the same manner as recorded ones. In each box, the lower trace is observed and the upper trace is simulated. Five selected stations are, top to bottom: PAC and LDM (rock) and PAR, SSU and SYL (deep soil/basin). Note that the latter three stations represent widely differing azimuths from epicenter. The general appearance and amplitudes match acceptably; however, the observed motion at rock stations is somewhat more spiky (non-Gaussian) than the simulated one.

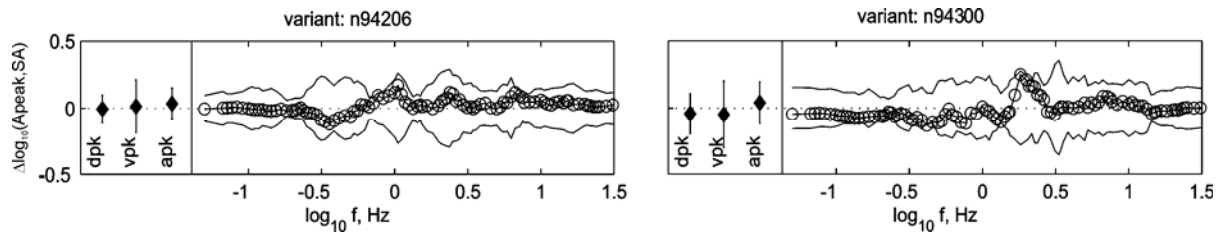


Figure 10. The misfit of horizontal peak and spectral amplitudes over 18 stations, for two simulated variants: 206 and 300. Misfit values are the differences (simulated minus observed) between \log_{10} peak displacements, velocities and accelerations (left box in each graph), and for \log_{10} pseudo response accelerations (right box). For all differences, average values over two horizontal components are shown. Standard deviations over 18 stations for the same data are shown, as error bars for amplitudes, and as a corridor around zero level for spectra.

and averaged over 18 stations (Fig. 10, Table 2). Numerical results for $\Delta \log_{10}(A)$ of the variant 206 are given in Table 2 with averages and rms deviations for all 10 variants. All results in Fig. 10, Table 2 and in all subsequent tables reflect the analysis of average values over two horizontal components of a station. (Note that for this reason the estimates of uncertainty obtained below must be multiplied by 1.2-1.4 to become comparable with the results of analysis of individual components of motion). For compactness, in Table 2 we cite values of $\Delta \log_{10}(\text{PRA})$ averaged over several frequencies. Namely, the values in line A are averages over all 25 frequencies; and in lines XL, L, M, and S, averages are given over frequency bands 0.1 to 0.3 Hz (“extra long” period), 0.31 to 1.5 Hz (long period), 1.51-5 Hz (medium period) and 5.1-20 Hz (short period), respectively. In lines a, v and d, the results of similar processing are given for peaks of acceleration, velocity, and displacement, respectively. Considering parameters of Table 2, one should have in mind that each real published observed record corresponds to a particular orientation of the instrument, and have been passed through component-specific band-pass filter (in order to get rid of unreliable parts of spectrum). We apply appropriate rotation of coordinate system and similar filter to the corresponding simulated record; thus, we always use comparable peak amplitudes.

The 206 column contains residuals (averaged over stations) for the selected variant 206. The AV column contains average residual over ten simulated variants (note that 0.05 in log₁₀ units equals 12% change; that is, most misfit estimates do not exceed 10%). The SV column contains inter-variant rms deviation for station averages of each variant. The S_{is} column contains interstation rms deviation, again averaged over 10 variants (values for the variant 206 are close to these). The dispersion of results among variants is analyzed in more detail later. At this stage, one can see that misfit estimates, both for individual variant 206 and average over variants, are well within the inter-station scatter, and less than 15% in terms of amplitude value, suggesting that the simulation procedure can be considered as consistent.

Table 2. Misfit of simulated ground motion parameters for the case of the 1994 Northridge earthquake. Given are $\Delta\log_{10}$ values (simulated minus observed) for response spectral and peak amplitudes

	206	AV	SV	S _{is}
A	0.022	0.028	0.075	0.179
XL	-0.016	0.040	0.102	0.182
L	-0.012	-0.021	0.090	0.223
M	0.057	0.037	0.070	0.189
S	0.041	0.056	0.062	0.146
a	0.036	0.023	0.072	0.141
v	0.015	0.018	0.098	0.128
d	-0.006	0.044	0.107	0.187

On the whole, the results of comparison can be considered as quite satisfactory. Bazurro et al. (2004) studied how well the results of our simulation, and also of six more techniques for simulation of ground motion can emulate peaks of linear and especially non-linear response of SDOF to observed motion. Among seven simulated data sets, the technique described above was the only one that produced realistic results over wide (0.25-10 Hz) frequency band analyzed.

4. UNCERTAINTY ANALYSIS

4.1 General review of factors that contribute to variability

For a given site, we can review the causes of variability/uncertainty of ground motion that are simulated within our procedure. Effects of parameters that are not simulated (hopefully not very large) cannot be studied, and shall contribute to misfit of simulation. These causes of variability can be divided into the following groups:

Group A: causes that can be expressed through input parameters of simulation. Their values can vary for natural reasons (producing aleatoric uncertainty), or they can be definite in principle, but known with limited accuracy (epistemic uncertainty). The related uncertainty of result can be treated either

through fixing sets of variants for the parameters and using logical trees, or through assumption that probability distributions are known for these parameters.

A1: source-related parameters/functions

1. Location (for moment and/or energy centroid or earthquake fault center); moment magnitude; fault orientation and slip direction.
2. Source size (area, length, width, depth range), stress drop value. Relative position of nucleation point. Average rupture velocity. Rise time.
3. Parameters that control the final slip function.
4. Parameters that control the intensity of non-Gaussian, heavy-tailed acceleration spikes
5. Far-field spectral shape, e.g. “omega-square”, parametrized through corner frequency and the deviation of the stress drop from the regional average value.

A2: propagation-related:

1. A particular 3D structure of the territory in question including site geology. Within our technique, only the effect of uncertainty of the assumed 1D velocity profile can be analyzed.
2. Site-specific kappa.

Group B: Effectively random, purely aleatoric factors. No reasonable prediction for many details of future fault motion can be expected, and their variability can be treated in practice only from a statistical viewpoint. Correspondingly, their effect is simulated through Monte-Carlo approach, and one can represent this effect through such parameters as mean, variance, or a set of quantiles (fractiles). Each of these factors is controlled by an independent random seed. At present, the following factors are treated in this way:

1. Particular final slip distribution
2. Time history of slip at a particular location on the fault
3. Variations in rupture velocity

We shall also review two more groups of factors that are not analyzed.

Group C. Potentially controllable factors whose effects were considered to be secondary for the moment. These include: variations of *mean* rise time for entire fault, variability of the *local* rise time value over the fault area, variations of spectral properties of radiation over the fault, errors in the estimation of the regional spectrum scaling law. Possible complete stopping of the rupture and its further restart is not permitted, and effect of this factor is not studied. Similarly, multiple-segment and curved ruptures are not permitted as well. Variability of slip direction over a fault is ignored. Scattering contribution to propagation effects is not considered. For a considerable part of such assumedly secondary factors, numerical estimates are of low accuracy, giving an additional obstacle to their use in practical strong

motion prediction. Of course, the above list of “secondary” factors is highly subjective. We plan to incorporate some of them into later versions of the simulation procedure.

Group D. There are manifestations of variability that are covered neither by our model nor by any alternative simulation approach known to us. This residual variability is related to factors whose modeling is near to impossible at present, or whose nature is obscure. These factors can be seen as prominent, anomalous “bright spots” and “shadows” of strong motion amplitudes, with characteristic distance scales from tens meters to kilometers. Known cases of “Tarzana” and “Santa Monica” records of Northridge earthquake represent some prominent examples of such variations. This variability includes an approximately lognormal component, with rms deviations of the order of magnitude $0.15-0.3 \log_{10}$ units (depending on the actual variability of local geology and topography), and also anomalous, “heavy-tailed” or “outlier” component illustrated by the two mentioned records of Northridge event. Many such anomalies were discovered during mapping the intensity of old earthquakes.

One more kind of “anomalies” is related to isolated high-amplitude acceleration and velocity spikes like ones observed for Nahanni 1986 and Petrolia 1992 earthquakes. Although they can be easily emulated within the presented procedure by means of artificial increase of CV_r parameter, this is only an ad hoc solution, not completely adequate for prediction of future earthquake ground motion. In general, Group D may produce a significant contribution to the full uncertainty of any strong motion prediction. What is important, this contribution, if treated statistically, is heavy-tailed non-Gaussian.

4.2 Preliminary uncertainty estimates for the 1995 Northridge earthquake case. General approach

In the following we construct variability/uncertainty estimates for the already simulated single prediction, as if we knew nothing about the true solution. This was done again for the set of 18 stations, and we analyzed average misfit over this station set. According to the discussion in the previous section, the factors were analyzed in the following manner. Five aleatoric and random factors (see “Group B” above) were categorized as Type 1 factors and analyzed in terms of mean and rms deviation of the $\log_{10}(\text{PRA})$. (PRA=pseudo response acceleration). Three of these factors characterize intrinsic model uncertainty; they are represented in simulation as random seeds. Each of them defines a particular realization of, respectively, (1) the final slip function, (2) the set of subsurface time functions and (3) the rupture propagation history. Two more factors were, intrinsically, parametric, but were treated as random ones, namely (4) the position of the nucleation point, and (5) the value of the mean rupture velocity. For each of these two factors, an appropriate probability distribution was fixed, and both were randomized using two more random seeds. In our opinion, these five factors are major fault-related causes of uncontrollable, aleatoric variability. For each parameter of Type 1, we simulated 16 variants of strong motion, varying only this parameter, and keeping all others fixed. In this way we could estimate the mean and variances related to each parameter separately. Note that if the effect of these parameters

were statistically independent, their contributions to the total variance would be additive. It was interesting to check this property. Towards this end, we also generated 16 variants with all five random seeds “active” simultaneously. The mean and rms deviation of this case can be compared to those expected assuming independence of factors.

We combined factors tractable as aleatoric or epistemic depending on the level of our understanding as Type 2 factors (see “Group A” above)/ We analyze their effect on $\log_{10}(\text{PRA})$ by means of sensitivity approach. Again, factors were analysed one by one. To estimate sensitivity coefficients we used a reference group of eight simulated variants, and determined the effect of variation of each single factor (i.e., sensitivity) using three levels of the factor: the reference one and two additional ones. With variance of a factor and sensitivity value at hand, we can predict the effect of a factor on the parameters of strong motion using the assumption of linearity. This was done; but the results must be treated with caution because we did not study effects of interaction among factors. Nevertheless, our results can give the preliminary estimates that clarify relative importance of factors.

The analysis included five Type 2 factors that are intrinsic to the source:

1. Stress drop value.
2. The DV parameter that define the range of variations of rupture velocity
3. The exponent s in the power law that defines the power spectrum of the final slip.
4. CV_r parameter
5. CV_{xy} parameter

To this group, we add the value of the scalar seismic moment M_0 .

There are also “external” factors that are related to the position and orientation of the finite source in 3D space. These factors (“Type 3”) include: the epicenter and depth for the center of the fault rectangle, strike, dip and rake angles. These parameters have two important properties. First, the effect of their variation on the $\log_{10}(\text{PRA})$ can vary significantly (including its sign) depending on the position of a station, so that the estimates of this effect as manifested for a particular station or set of stations should be viewed only as an example, and have no generality. Second, this effect can be estimated analytically beforehand, (though with a limited accuracy) using the known geometry of the subsource grid and the radiation pattern of each point-source double couple. For these reasons we did not pay much attention to this group of parameters. Nevertheless, with the aim of demonstration we studied the sensitivity of the station-averaged $\log_{10}(\text{PRA})$ for four parameters of this group, namely the fault dip, strike and rake, and the fault rectangle center depth H_{rec} .

No analysis of medium-related factors was carried out. The main reason is that we see the major component of medium-related variability to be related not to the errors of the average model, but to the actual 3D structure of the medium, including both “lateral velocity anomalies” of considerable size and small size heterogeneity. We have no means to reliably estimate such effects in any apriori way; however, they can be reliably estimated empirically. Indeed, medium-related uncertainty manifests itself as

a main component of inter-station variability, expressed as rms residual of fit of predicted vs. observed amplitudes. Note that this estimate is also not very general because in different geological environments, highly varying levels of medium variability can be expected.

4.3 Uncertainty estimates for “Type 1” parameters

In the following Table 3, the results of analysis of 16 variants with different random seeds are given. Table 3 is constructed in the same way as Table 2, with similar meaning of rows.

Table 3. Effects of five random factors: rms deviation of $\log_{10}(\text{amplitude})$

	slip	time fun.	V_{rup} variat.	V_{rup} mean value	[xy] nucleat.	5 effects added	5 effects combined
A	0.0475	0.0216	0.0420	0.0667	0.0315	0.0996	0.0889
XL	0.0574	0.0298	0.0728	0.1081	0.0709	0.1618	0.1372
L	0.0564	0.0473	0.0583	0.0840	0.0342	0.1305	0.1284
M	0.0402	0.0441	0.0253	0.0582	0.0174	0.0888	0.0650
S	0.0519	0.0254	0.0306	0.0426	0.0225	0.0812	0.0697
a	0.0542	0.0261	0.0474	0.0523	0.0270	0.0966	0.0746
v	0.0510	0.0422	0.0640	0.0794	0.0485	0.1309	0.1047
d	0.0615	0.0256	0.0682	0.0670	0.0756	0.1389	0.1244

In processing $\log_{10}A$ data, values were averaged over stations, and then station averages were analyzed. In the columns of Table 3, the estimates are given of the standard deviation of the station averages among 16 variants. These values characterize intrinsic variability among individual realizations of earthquakes. Each of the columns characterize one of the following random factors:

1. Final slip distribution over the fault area. Its realizations are controlled by a random seed, whereas its general properties are defined by the s and CV_{xy} parameters analyzed later.

2. Subsource time history functions. These are segments of non-stationary noise with the duration defined by the value of the rise time. The particular realization for their entire set is generated from a single random seed.

3. Individual random details of the time history for rupture velocity. In the version used, rupture fronts are circular, and there is a separate random seed that defines the particular sequence of rupture velocity values that define consecutive positions of the rupture front. The range of individual rupture velocity values is determined by DV parameters whose value was set equal to 0.8 in this particular analysis.

4. Mean value of rupture velocity. This factor is essentially deterministic; we however decided to randomize it. We assumed that rupture velocity acquires value within the range 2.16-3.24 km/s (Mach number 0.6-0.9), following the uniform distribution law. The selection of this particular range for Mach number is based on the general seismological evidence.

5. Position of the nucleation point. This factor, though deterministic in essence, was again treated as a random one. To randomize it, we assumed that the nucleation point may be located anywhere within the

deepest 30% of the fault area, with uniform probability density. This particular mode of randomization for the nucleation point position is a formal representation of common seismological evidence that nucleation points are typically located somewhere within the lower part of the dip-slip fault.

Regarding relative importance of factors, one can see from Table 3 that the most significant factor among five analyzed is the mean value of rupture velocity. Randomness of slip and random velocity variations are also significant; and nucleation point position is less important. Effect of random seed in time histories of subsources is minimal. Note that low effect of nucleation point position is definitely not a general result; this fact is clearly associated to our constraining range for its position. Also note that the assumed degree of rupture velocity variation is probably too low; more realistic value might significantly increase the related effect.

We mentioned that we also tried to perturb all “random” factors simultaneously. Assuming independence of factors, one can predict their joint effect through addition of variances. Or, one can disturb all factors in parallel, so that the dependence between factors, may manifest itself. Results for each of these modes are given in the last two columns of Table 3. One can see no expressed differences; so that in this case, summation of variances is acceptable.

4.4 Uncertainty estimates for “Type 2” parameters

To understand effects of “Type 2” parameters on uncertainty, we, for each factor, proceed in the following way: (1) we estimate the value of sensitivity $d \log_{10}(\text{amplitude})/ d(\text{factor})$, (2) make some reasonable assumption about the value of rms variation of the factor, and then (3) multiply the two values. The product gives us a certain estimate for the contribution of the factor into complete uncertainty of amplitude. To determine sensitivity we select a reference level of a parameter and two levels above and below it. Sensitivity is estimated from finite difference, averaged over eight variants of random seeds analyzed.

1. Stress drop. The effect of stress drop $\Delta\sigma$ variation (at a given M_0) on amplitudes is twofold. First, increased $\Delta\sigma$ results in higher corner frequency and enhanced high-frequency energy. Second, the fault area and signal duration decrease, so that this energy is distributed over a smaller time span. Both factors imply the general increase of near-fault amplitudes. We select $\Delta\sigma = 60$ bar (6 MPa) as the reference value and two other values: 96 and 37.5 bar (1.6 times up and down from the reference, or ± 0.20 in \log_{10} units). The values of the derivative $d \log_{10}(\text{amplitude})/ d(\log_{10}(\Delta\sigma))$ are given in the first column of Table 4,

2. Coefficient of variation CV_i for amplitudes of delta-like spikes. The value of this parameter defines whether accelerograms will appear “Gaussian-noise-like” or will look “spiky” and have non-Gaussian, heavy-tailed statistics. The accepted reference value for this parameter is 0.5, producing a

moderately spiky behavior. We used two levels of CV_t , equal to 0.2 (almost Gaussian behavior) and 1.0 (expressed spiky behavior). Results show significant non-linearity: amplitudes increase approximately two times faster with positive change of CV_t . We selected conservative estimate of sensitivity ($d\log A/dCV_t$), based on the difference between levels 0.2 and 0.5; see table 4 for the result. Its unexpected feature is quite significant effect of non-Gaussianity on *low-frequency* response and peak *displacement*.

Table 4. Sensitivity estimates with respect to Type 2 factors

	$\log_{10}\Delta\sigma$	CV_t	CV_{xy}	s	DV
A	0.319	0.192	0.091	≈ 0	≈ 0
XL	0.411	0.042	0.076	≈ 0	≈ 0
L	0.374	0.180	0.061	≈ 0	≈ 0
M	0.233	0.254	0.072	≈ 0	≈ 0
S	0.251	0.222	0.136	≈ 0	≈ 0
a	0.314	0.235	0.062	≈ 0	≈ 0
v	0.417	0.182	0.100	≈ 0	≈ 0
d	0.389	0.090	0.104	≈ 0	≈ 0

3. Coefficient of variation CV_{xy} for the values of final slip distribution (or subsurface seismic moment). This parameter defines how strongly oscillating will be the simulated final slip function. At the reference case, we set $CV_{xy}=0.5$. Two more levels of CV_{xy} were tried, namely $CV_{xy}=0$ (zero variation of slip, the classic Haskell’s constant-final-slip case), and $CV_{xy}=0.9$. Again, only the difference between lower cases, 0 and 0.5, was used to determine sensitivity, see Table 4.

4. The exponent s in the power law that defines the power spectrum of the final slip. This parameter defines the balance between low and high wavenumbers in the spectrum of the final slip. At $s=0$, flat spectrum will be obtained, and the final slip function will represent high-wavenumber “white noise” with no distinct structural elements like “asperities”. At the reference case, we set $s=1.5$. Two more levels of s were tried, namely $s=1.0$, and $s=2.2$. The results were unexpected: no clear trend is seen, and amplitudes are maximal around $s=1.5$. Also, the value of the change is small (order of 0.01 in \log_{10} units). Therefore, this factor can be treated as insignificant and excluded from further analysis.

5. The range of variations for the rupture velocity (DV parameter). This parameter controls the scale of rupture velocity variations; with $DV=0$, such variations disappear and cannot have any effect. In a manner similar to the previous subsection we use the value $DV=0.8$ as the reference case, and check two more levels of DV , namely, 0.0 and 1.0. The results were unexpected: the estimates of the effect were near-zero (order of 0.01), and showed no systematic picture. This is indicated symbolically as the column of “ ≈ 0 ” in Table 4. This result probably means that the assumed range for DV values are unrealistically small, or that our accepted scheme of perturbing of timing of subsources is inefficient. Detailed analysis is left for future.

6. Seismic moment variation. It is a matter of choice to include seismic moment or moment magnitude into the list of factors of uncertainty. In this study, we considered M_w as fixed. For general estimates, one can believe that the value of sensitivity to this factor, $d\log_{10}(\text{amplitude})/d\log_{10}(M_0)$, shall be bracketed between 0.2-0.3 at high frequencies and 0.5-0.67 at low frequencies. Thus, for a minimum reasonable uncertainty in M_w , equal to 0.1, uncertainty in $\log_{10}(A)$ shall be typically between 0.04 and 0.1.

4.5 Uncertainty estimates for “Type 3” parameters, and joint effect of Type 2 and Type 3 factors on uncertainty

For Type 3 parameters, analysis of sensitivity is much less interesting because their effect on amplitudes is deterministic and predictable. Also, these effects have no generality because they strongly depend on the particular fault and slip geometry and station positions. Thus we shall make only short comments. We analyzed the effects of fault center depth, and of angles of strike, dip and rake. The effect of depth was predictable, with sensitivity $d \log A/dH \approx -0.018$ estimated over the depth range 9-16 km. The effect of dip change was clear increase of amplitude with dip angle. This effect is most enhanced at low frequency: up to +0.08 log10 units of increase for the dip change from 30° to 50°. At high frequency, the amplitude change decreases down to +0.025 log10 units. Changes of strike by $\pm 10^\circ$ and of rake by $\pm 20^\circ$ make negligible effect on amplitudes.

Now we can tentatively estimate the effect of Type 2 and Type 3 parameters on uncertainty using the estimated sensitivities, ignoring small effects of parameters s , DV , strike and rake. We assume epicenter to be fixed. For other parameters, we assume that their uncertainty, be it intrinsically aleatoric or epistemic, can be represented as independent random factor with normal distribution law. We ascribe certain tentative values to standard deviations to the parameters, see the σ_i line of Table 5. For stress drop, we assume minimal reasonable errors. For H_{rec} and dip, reasonable typical values are assumed. For CV_t and CV_{xy} , the assumed values formalize our subjective uncertainty regarding their true values.

Table 5. Estimates of rms deviations of log amplitudes related to individual factors, and to joint effects

	$\log_{10}\Delta\sigma$	CV_t	CV_{xy}	H_{rec}	dip	S_{23}	S_{123}	S_{tot}
	0.1	0.15	0.15	2.5km	10°			
A	0.031	0.028	0.013	0.045	0.024	0.068	0.111	0.211
XL	0.041	0.006	0.011	0.038	0.041	0.071	0.154	0.238
L	0.037	0.027	0.009	0.045	0.021	0.068	0.145	0.266
M	0.023	0.038	0.010	0.045	0.005	0.064	0.091	0.209
S	0.025	0.033	0.020	0.041	0.021	0.065	0.095	0.174
a	0.031	0.035	0.009	0.057	0.015	0.076	0.106	0.176
v	0.041	0.027	0.015	0.053	0.033	0.081	0.132	0.184
d	0.038	0.013	0.015	0.045	0.034	0.071	0.143	0.235

Multiplying these five numbers by the values of sensitivities of Table 4, we obtain five single-factor standard deviations given in the lower lines of Table 5 (first five columns). In the column S_{23} we give

the standard deviation obtained, through usual summation of variances, for joint action of five factors of Types 2 and 3. Note that this result is somewhat formal because it strongly depends on the particular choice of the values of uncertainties for individual parameter, selected subjectively. Then we can combine this result, in a similar manner, with the last column of Table 3, obtaining the joint effect of all three discussed groups of source-related factors, denoted S_{123} .

The contributions to uncertainty from imperfect description of the medium were derived from the dispersion of amplitude residuals (simulated minus observed) over 18 stations used, see the column S_{is} of Table 2. Although these residuals inevitably include some unaccounted source-related factors, role of medium-related uncertainty must be dominating. At last, combining source and medium contributions, we obtain final rms deviations $S_{tot} (=S_{123}^2+S_{is}^2)^{0.5}$ that characterize total uncertainty. These final estimates, of 0.18-0.26 log10 units of full uncertainty in terms of rms deviation, looks quite realistic for the average over two components. It is interesting to note that highest-frequency signal component, reflected in lines S and a, has the lowest source-related uncertainty, whereas the lowest-frequency signal uncertainty (lines XL, L and d) is the largest. Medium-related uncertainty shows less frequency dependence, and again the largest scatter is seen for the lower-frequency component of the signal.

Now we can make preliminary ranking for the factors of uncertainty, on the basis of relative contribution to joint variance. The most important single factor in uncertainty is the station-related term, probably manifesting both site geology effects and path-related effects like “focusing” etc. Among other factors, the groups of random seeds (“Type 1,” representing intrinsic model uncertainty) and the group of parametric factors (“Type 2” plus “Type 3”) seem to make approximately equal contributions. Among random seeds, the contribution of mean rupture velocity (treated as a random factor here) is the largest, representing its importance in forming the directivity effects. Second in this group is the contribution of random final slip distribution over fault area. As for absolute values, our estimates of uncertainty are based mostly on assumptions of minimum uncertainty of parameters, and thus must be treated as “optimistic” or “less conservative”.

5 CONCLUSION

Determination of probable ground motion from scenario earthquake, with adequate brackets on the parameters of this motion, is a complicated problem. In the presented case study we give preliminary results of the application of a new advanced technique for simulation of strong motion and estimating its uncertainty. The technique is based on the representation of the source as a set of point subsources. We created a simulated data set that satisfactory imitates the observed strong-motion data set for Northridge (1994) earthquake (epicentral stations only). We also have shown how our simulation technique can be applied to characterize the uncertainty of the results of a simulation, and shed some light on the relative importance of various contributions to uncertainty. Figures are to be numbered consecutively with the caption below.

Acknowledgments

The work was supported by the SAND group of the Abdus Salam International Centre for Theoretical Physics, Trieste, Italy. Authors are indebted to Giuliano Panza who proposed the study. Discussions with him, Fabio Romanelli and Franco Vaccari were highly valuable. Analysis of uncertainty was proposed and facilitated by Organizing Committee for Treasure Island prediction exercise; they also kindly provided station characteristics and preprocessed observational data.

REFERENCES

- Aki K. (1967). Scaling law of seismic spectrum: *J. Geophys. Res.* 72, 1217-1231.
- Alekseev A.S and Mikhailenko B.G. (1980). The solution of dynamic problems of elastic wave propagation in inhomogeneous media by a combination of partial separation of variables and finite-difference method. *J. Geophys.* 48, 161-172.
- Anderson J.G. and S.E. Hough (1984). A model for the shape of the Fourier amplitude spectrum of acceleration at high frequencies, *Bull. Seismol. Soc. Am.*, 74, 1969-1993.
- Andrews D. J. (1980). A stochastic fault model. 1. Static Case. *J. Geophys. Res.*, 78, p. 3867-3877.
- Bazzurro P., Sjoberg, B. and Luco, N. (2004), Post-Elastic Response of Structures to Synthetic Ground Motions. Techn. Report AT2, for PEER Lifelines Program project 1G00, *AIR Worldwide Co.*, San Francisco,
- Boatwright J. (1982). A dynamic model for far-field acceleration, *Bull. Seism. Soc. Am.* 72, 1049–1068.
- Boore D. M. (1983). Stochastic simulation of high-frequency ground motions based on seismological models of radiated spectra, *Bull. Seism. Soc. Am.* 73, 1865–1894.
- Brune J. N. (1970). Tectonic stress and the spectra of seismic shear waves from earthquakes, *J. Geophys. Res.* 75, 4997–5009.
- Fatyanov A.G. and Mikhailenko B.G. (1988). A method for calculating non-stationary wave fields in anelastic layered media. *Doklady AN SSSR*, 301, 834-839. (In Russian).
- Gusev A.A. (1983). Descriptive statistical model of earthquake source radiation and its application to an estimation of short-period strong motion. *Geophys. J. Roy. Astr. Soc.*, 74, 787-808.
- Gusev A.A. (1989). Multiasperity fault model and the nature of short-period subsources. *Pure Appl. Geophys.*, 130, 635-660.
- Gusev A.A. (1996). Peak factors of Mexican accelerograms: evidence of non-Gaussian amplitude distribution. *J. Geophys. Res.* 101, 20083-20090.
- Hanks T. C. and R. K. McGuire. (1981). The character of high-frequency strong ground motion, *Bull. Seism. Soc. Am.* 71, 2071–2095.
- Hartzell S. H. (1978). Earthquake Aftershocks as Green's Functions, *Geophys. Res. Lett.* 5, 1–4.
- Haskell N. A. (1964). Total energy and energy spectral density of elastic wave radiation from propagating faults, *Bull. Seismol. Soc. Am.*, 54, 1811-1841.

- Haskell N.A. (1966). Total energy and energy spectral density of elastic wave radiation from propagating faults. II. A stochastic fault model. *Bull. Seism. Soc. Am.*, 56, 125-140.
- Heaton T.H. (1990). Evidence for and implications of self-healing pulses of slip in earthquake rupture. *Phys. Earth Planet. Inter.*, 64: 1-20.
- Irikura K. (1986). Prediction of strong acceleration motions using empirical Green's function, *Proc. 7th Japan Earthq. Symp.* 151–156.
- Joyner W.B. (1984). A scaling law for the spectra of large earthquakes, *Bull. Seism. Soc. Am.*, 74, 1167-1188.
- Koyama J. (1985). Earthquake source time-function from coherent and incoherent rupture, *Tectonophysics* **118**, 227–242.
- Pavlov V.M. (2001). Calculation of synthetic seismograms in layered elastic media. *Abstracts 3rd Conf. "Problems of seismicity of the Far East"*, , *Khabarovsk* , 11. (In Russian).
- Papageorgiou A.S. and Aki K. (1983). A specific barrier model for the quantitative description of inhomogeneous faulting and the prediction of the strong ground motion. I. Description of the model, *Bull. Seismol. Soc. Am.*, 73, 693-722.
- Papageorgiou A. S. and Aki K. (1985). Scaling law of far-field spectra based on observed parameters of the specific barrier model, *Pure Appl. Geophys.* 123, 354–374.
- Somerville P., K. Irikura, R. Graves, S. Sawada, D. Wald, N. Abrahamson, Y. Iwasaki, T. Kagawa, N. Smith and A. Kowada (1999). Characterizing crustal earthquake slip models for the prediction of strong motion, *Seism. Res. Lett.* **70**, 59–80.
- Takeuchi H. and Saito M., (1972). Seismic surface waves, in *Methods in Computational Physics* 11, edited by B. A. Bolt, 217-295, *Academic Press*, New York,.
- Wald D.J., Heaton T.H and Hudhut K.W. (1996). The slip history of the 1994 Northridge, California, earthquake determined from strong ground motion, teleseismic, GPS, and leveling data, *Bull. Seism. Soc. Am.*, 86, S49-S70.